Oil & Gas Science and Technology – Rev. IFP Energies nouvelles (2016) **71**, 15

DOI: 10.2516/ogst/2014033

Effect of Pilot Injection Timings on the Combustion Temperature Distribution in a Single-Cylinder CI Engine Fueled with DME and ULSD

Joonho Jeon[1], Yong Hee Park[2], Sang Il Kwon[2] and Sungwook Park[3]*

[1] Department of Mechanical Convergence Engineering, Graduate School of Hanyang University, Seoul 133791 - Republic of Korea
[2] National Institute of Environmental Research, Incheon 404170 - Republic of Korea
[3] School of Mechanical Engineering, Hanyang University, 17 Haengdang-dong, Seongdong-gu, Seoul 133791 - Republic of Korea
e-mail: parks@hanyang.ac.kr

* Corresponding author

Abstract — *Many studies of DiMethyl Ether (DME) as an alternative fuel in Compression-Ignition (CI) engines have been performed. Although diverse DME engine research has been conducted, the investigation of combustion behavior and temperature distribution in the combustion engine has not progressed due to the fact that there is no sooting flame in DME combustion. In order to investigate the combustion characteristics in this study, the KIVA-3 V code was implemented to research various pilot injection strategies on a single-cylinder CI engines with DME and Ultra-Low-Sulfur Diesel (ULSD) fuels. The combustion distribution results obtained from the numerical investigation were validated when compared with the measurement of flame temperature behaviors in the experimental approach.*

This study showed that long intervals between two injection timings enhanced pilot combustion by increasing the ambient pressure and temperature before the start of the main combustion. Different atomization properties between DME and ULSD fuels contributed to the formation of a fuel-air mixture at the nozzle tip and piston lip regions, separately, which strongly affected the temperature distribution of the two fuels. In addition, the pilot injection timing played a vital role in regard to ignition delay and peak combustion temperatures. Exhaust emissions, such as NO_x and soot, are related to the local equivalence ratio and temperature in the combustion chamber, also illustrated by the contrary result on a Φ (equivalence ratio) – T (temperature) map.

Résumé — **Effet des réglages à l'injection sur la répartition de la température de combustion dans un moteur monocylindre à allumage par compression et alimenté avec du DME et du Diesel à ultra basse teneur en soufre** — De nombreuses études concernant le diméthyléther (DME) en tant que carburant alternatif dans des moteurs à allumage par compression (CI) ont été effectuées. Bien que différentes recherches sur les moteurs DME aient été réalisées, l'étude du comportement à la combustion et des répartitions de température dans le moteur à combustion n'a pas progressé du fait qu'il n'existe aucune flamme d'encrassement lors de la combustion du DME. Afin d'étudier dans le présent travail les caractéristiques de combustion, le code KIVA-3 V a été appliqué pour rechercher différentes stratégies d'injection pour des moteurs CI monocylindres avec comme carburants du DME et du Diesel à teneur en soufre

ultra basse (ULSD). Les résultats obtenus dans l'étude numérique de la distribution de la combustion, ont été validés par rapport aux mesures de la température de flamme de l'approche expérimentale.
Cette étude a montré que de longs intervalles entre deux réglages de l'injection amélioraient la combustion en augmentant la pression ambiante et la température avant le début de la combustion principale. Différentes propriétés d'atomisation entre les carburants DME et ULSD ont contribué à la formation séparée du mélange combustible-air à la pointe du gicleur et dans des zones du piston, ce qui affecte fortement la répartition des températures des deux carburants. En outre, le réglage à l'injection a joué un rôle essentiel quant aux retards à l'allumage et aux pics de températures de combustion. Les émissions à l'échappement, tels que les NO_x et les suies, sont liées au rapport d'équivalence local et à la température dans la chambre de combustion, comme cela est illustré par un résultat contradictoire sur une cartographie Φ (rapport d'équivalence) – T (température).

NOMENCLATURE

ALE	Arbitrary Lagrangian-Eulerian
ATDC	After Top Dead Center
BTDC	Before Top Dead Center
CA	Crank Angle
CI	Compression-Ignition
deg.	Degree (^{o})
DICI	Direct Injection Compression-Ignition
DME	DiMethyl Ether
EGR	Exhaust Gas Recirculation
HRR	Heat Release Rate
HSDI	High-Speed Direct Injection
IMEP	Indicated Mean Effective Pressure
KH	Kelvin-Helmholtz
$P_{inj.}$	Injection pressure
Φ	Equivalence ratio
RNG	ReNormalization Group
RT	Rayleigh-Taylor
T	Temperature
$\tau_{inj.}$	Injection timing
TDC	Top Dead Center
ULSD	Ultra-Low-Sulfur Diesel

INTRODUCTION

As the quality of human life increases, many people are concerned with their health and the environment. Naturally, they try to improve their life conditions and keep their surroundings clean. As a result, very strict regulations have emerged. These regulations have led to highly technical evolution in various industrial fields. For instance, the Euro VI regulation has high standard values for noxious emissions emitted from Diesel engines. Although Diesel engines are able to generate high power, harmful emissions such as HydroCarbons (HC), Carbon monoxide (CO) and soot are also made. Therefore, many researchers and engine manufacturers have developed various technologies; combustion strategies, after-treatment devices, EGR systems, and alternative fuels to allow engine manufacturers to meet stringent standards. Among the various methods used for the reduction of noxious emissions, alternative fuels have been highlighted because they can possibly reduce both emission problems and a dependency on fossil fuels. DME fuel is one of the best alternative fuels for the Compression-Ignition (CI) engine due to its high self-ignition characteristics, oxygen content, and no soot combustion [1].

Numerous experiments for the adaptation of DME fuel to the CI engine have been conducted. Kim *et al.* [2] reported that DME combustion showed a higher Indicated Mean Effective Pressure (IMEP) and a better complete combustion process than those of Diesel fuels based on a constant energy. In addition, DME fuel showed a more stable combustion event than Diesel combustion. Due to the low lubricity and high evaporation rate of DME fuel, Sato *et al.* [3] designed a new type of injection system called a jerk-type in-line DME injection system, optimized for the light-duty truck engine. The DME engine with the jerk-type in-line system achieved better fuel consumption and lower emission levels than those of Diesel combustion under similar, sustained output conditions. DME fuel has a low energy density of about 55% of Diesel fuel, which requires a greater injection quantity and longer injection duration compared with Diesel fuel. Despite the increase in mass and injection duration, the DME engine exhausts a smaller amount of

NO_x (by 40%), CO_2 (by 15%) and extremely low THC levels. An *et al.* [4] reported that the high injection pressure of DME fuel using a common-rail injection system shows low energy consumption and active atomization characteristics. Although the increased injection pressure improved the combustion performance, it was indicated that high NO_x emissions were also generated because of the active combustion event. Moreover, with no soot combustion from DME fuel, it is easily possible to increase engine torque in low speed conditions.

DME combustion in the CI engine produces high engine performances and low emissions such as CO, HC and soot. However, it cannot be ignored that a significant concentration of nitrogen oxides is emitted from DME engines. In order to decrease NO_x emissions, various combustion strategies have been applied in the CI engine fueled with DME. Yoon *et al.* [5] studied the effects of pilot injection on DME combustion and emission in a single-cylinder Direct-Injection Compression-Ignition (DICI) engine. They discovered that DME pilot injection reduces the NO_x emission concentrations, along with other emissions (CO, HC). An investigation of the reduction of NO_x emissions using the DME engine with an EGR system was conducted by Song *et al.* [6]. Due to the fact that NO_x emissions are actively formed under high oxygen concentration and combustion temperature conditions, the EGR system suppressed both of these conditions, and thus the formation of NO_x emissions. Their research demonstrated the optimized EGR rate under the ESC test cycle to meet the Euro IV standards. In their study, the DME engine with an EGR system achieved lower NO_x emissions than the Euro IV limit, and suggested that an additional oxidation catalyst can also reduce CO and HC simultaneously. Among these methods to lower exhaust emissions, a pilot injection strategy is easily available in conventional Diesel engine fueled with DME without any modification.

However, there have been few detailed studies on the effects of the pilot injection on DME combustion. Therefore, this study focuses on DME combustion and emission characteristics under various injection regimes using the numerical approach. A previous study [7] carried out analytical research on the DME combustion and emission under single-injection conditions, and showed high prediction results as compared with experiments. The same simulation code and methods were used in the current research on the effects of the pilot injection timing. The numerical experiment analyzed the processes of the fuel-air mixture formation and combustion temperature distribution for combustion characteristics. For an analysis of emissions for DME and ULSD combustion, an Φ (equivalence ratio) – T (temperature) map was introduced.

1 NUMERICAL AND EXPERIMENTAL METHODOLOGIES

In the present study, a modified version KIVA-3 V release 2 which was a combination of the KIVA-3 V code [8, 9] and the CHEMKIN-II code [10], for spray and combustion simulations, respectively, was employed to enhance the prediction in the CI engine fueled with ULSD and DME fuels. In addition, an experiment with the AVL 5402 research single-cylinder engine was carried out for simulation validation. A multi-dimensional grid was generated based on the AVL 5402 engine.

1.1 Numerical Models for Engine Simulation

Spray which occurred inside the internal combustion engine was simulated by the KIVA-3 V code which takes the Arbitrary Lagrangian-Eulerian (ALE) method into account to solve the complex multi-phase flow. For the atomization calculation, the hybrid break-up KH-RT (Kelvin-Helmholtz and Rayleigh-Taylor) model [11] was applied. Also, the in-cylinder turbulent flow was considered with the modified ReNormalization Group (RNG) k-ε model [12]. For the interactions between spray droplets and the wall, a spray-wall interaction model was used, which enhanced the prediction of spray characteristics in this study. Although the KIVA-3 V code included fuel information of a gaseous DME fuel as a function of temperature, it was required to supplement it with the liquefied DME properties depending on factors such as temperature, viscosity, latent heat, and vapor pressure for the KIVA-3 V code. The liquefied DME properties were obtained from Teng *et al.*'s [13-15] and Teng and McCandless's [16] investigations and added to the fuel library. For the ULSD spray simulation, tetradecane ($C_{14}H_{30}$) was chosen as a surrogate fuel because tetradecane not only has analogous physical properties with those of the ULSD fuel, but also perfectly reproduces the behavior of ULSD spray in the combustion engine. The CHEMKIN-II code, which was a chemistry solver, coupled with the KIVA-3 V code was used for chemical reactions of fuels in their self-ignition and combustion processes. In the present study, a detailed DME mechanism [16], including 79 species and 351 reversible elementary reactions, was introduced to simulate ignition delay and fuel oxidation processes under various engine operating conditions. Because the mechanism contained low and high temperature reactions, the overall DME oxidation reactions could be depicted in the CI engine. The simulation for the ULSD combustion was conducted using the n-heptane (C_7H_{16}) mechanisms as the ULSD surrogate fuel, which was composed of 30 species and 65 irreversible

TABLE 1
Validation engine specifications

Item	Description
Engine type	Naturally-aspirated CI single cylinder engine
Injection system	*Bosch* common-rail direct injection system
Bore × stroke	85 mm × 90 mm
Displacement volume	510.7 cm^3
Compression ratio	17.1:1
Number of injection holes	5
Spray angle	142°

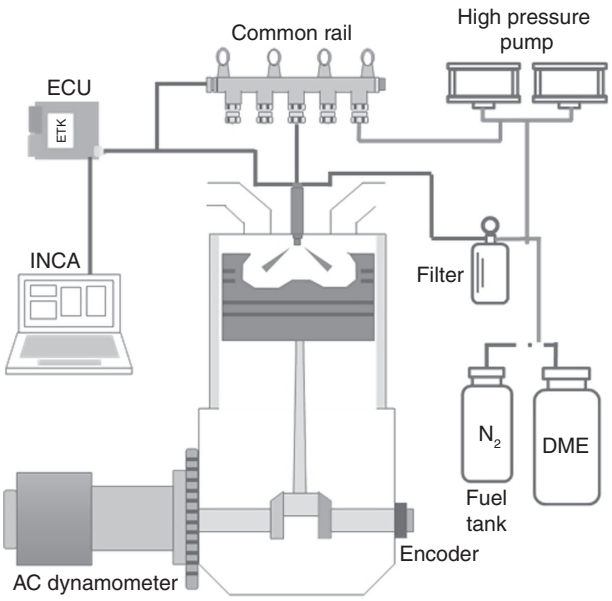

Figure 1
Schematic of experimental apparatus for the validation test.

reaction steps [17]. The emission models were also included for NO_x and soot emissions in the modified KIVA-3 V code. The reduced GRI NO mechanism [18] in combination with the detailed mechanism predicted the formation of NO_x emissions during the combustion processes. Additionally, a two-step soot model [19], which considered the competitive relation between formation and oxidation reactions, was used to compute the rate of soot emissions under various experimental conditions.

1.2 Experimental Apparatus

In order to validate the ULSD and DME fuel combustion and emission models, experimental research was performed using an AVL 5402 single-cylinder research engine equipped with a common-rail injection system. The detailed specifications and dimensions of the test engine are summarized in Table 1. The AVL single-cylinder compact test bed consists of a dynamometer (AMK DW 13-170-4), with a rated power up to 38 kW, and a rated torque up to 120 Nm, which is a three-phase asynchronous motor that can supply and absorb torque. A prototype ETAS engine control unit, which is an open-loop fuel injection strategy designed by AVL, was able to adjust the fuel injection parameters. The injection parameters such as the injection timing, pressure, and quantity could be altered respectively using INCA software that communicates with the ETAS system. In the fuel supply system, two high pressure pumps (HSF-300, *Haskel*) linked in parallel were used to stably supply fuel from a fuel tank to the common-rail, as seen in Figure 1. A HORIBA MEXA-554JKNOx exhaust gas analyzer was used to measure the CO (±0.06% vol.), HC (±12 ppmvol), and NO_x (±20 ppmvol) emissions under steady-state conditions. The ESC sensor, using a chemical method, estimates NO_x emissions and the HC and CO emissions are detected by the non-dispersive infrared ray method. In addition, the soot meter (Micro Soot Sensor, *AVL*) determined the soot concentration directly using the photo-acoustic measurement method (accuracy of ~5 $\mu g/m^3$). To visualize the combustion behavior and temperature distribution, a visualization system was introduced in this research. The visualization system consists of two parts: endoscope visualization equipment (Visioscope, *AVL*) and an image post-processing program (ThermoVision, *AVL*). The Visioscope is composed of an endoscope, CCD camera (1 280 × 1 024 pixels), and light unit. The endoscope was installed on the cylinder head with the CCD camera, and performed electric recording of the processes that took place in the combustion engine. The CCD camera and light unit were synchronized with a crank angle encoder (365C, *AVL*) to capture combustion images at an exact timing (1 CA resolution). The ThermoVision program allowed captured images to calculate flame temperature using electromagnetic radiation [20].

1.3 Experimental Procedures

The numerical experiment conditions were fixed to validation test conditions which were obtained from a single-cylinder CI engine. The injection timing was expanded from one condition to three main timings and seven pilot timings for DME and ULSD fuels.

Detailed test conditions were tabulated in Table 2. In the validation test, the two test fuels matched the same power condition. Fuel injection quantities used the same value as the experimental results.

2 RESULTS AND DISCUSSION

2.1 Model Validation

For an accurate prediction of multi-injection cases in the KIVA/CHEMKIN code, a comparison between experimental and numerical results was conducted. The two different injection conditions; single-injection and double-injection cases were chosen for validation with regard to the combustion pressure, heat release rate, and temperature distribution. The engine operating conditions for the validation were 1 500 rpm engine speed, 50 MPa injection pressure, and 18 Nm engine load. Under theses engine conditions, test fuels were injected at BTDC 60 CA and BTDC 10 CA, respectively. The computational grid modeled only one-fifth of the AVL 5402 research single-cylinder engine based on symmetry assumptions to reduce computation time.

TABLE 2
Detail simulation test conditions

Description		Conditions
Fuel		DiMethyl Ether (DME), Ultra-Low-Sulfur Diesel (ULSD)
Injection pressure (MPa)		50
Injection strategy		Pilot injection, main injection
Pilot injection quantity (mg)		2
Main injection quantity	DME (mg)	24.5
	ULSD (mg)	13.5
Pilot injection timing (BTDC, CA)		30, 40, 50, 60, 70, 80, 90
Main injection timing (BTDC, CA)		5, 10, 15
Engine speed (rpm)		1 500

The combustion pressure and the heat release rate for all validation cases are illustrated in Figure 2. In the ULSD case, the calculated pressure was predicted accurately compared with the measured pressure. Although the heat release rate shows a slight difference between the simulation and the experiment, this is because KIVA did not reflect the heat transfer effect at the cylinder wall. This effect is also observed in the DME combustion case. For the heat release rate of the DME simulation, the overall heat release rate was overestimated compared with the measured one. However, the peak pressure trends showed good agreement with the experimental results. The ignition delay of the DME case in the simulation was a little slower than that of the measured result. This is because a delayed first combustion was caused by the pilot injection, which led to the disagreement of the main combustion starting points with the experiment. On the other hand, the ULSD pilot combustion started earlier, raising the combustion pressure condition before the main combustion. Thus, the main combustion event

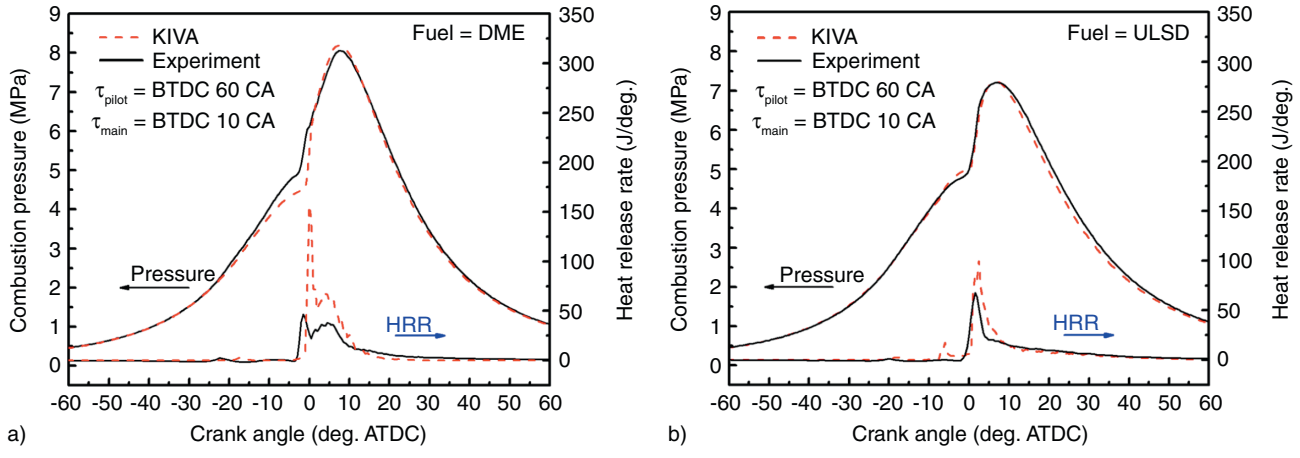

Figure 2
Combustion characteristics of a) DME and b) ULSD fuels in the comparison between the simulation and experiment.

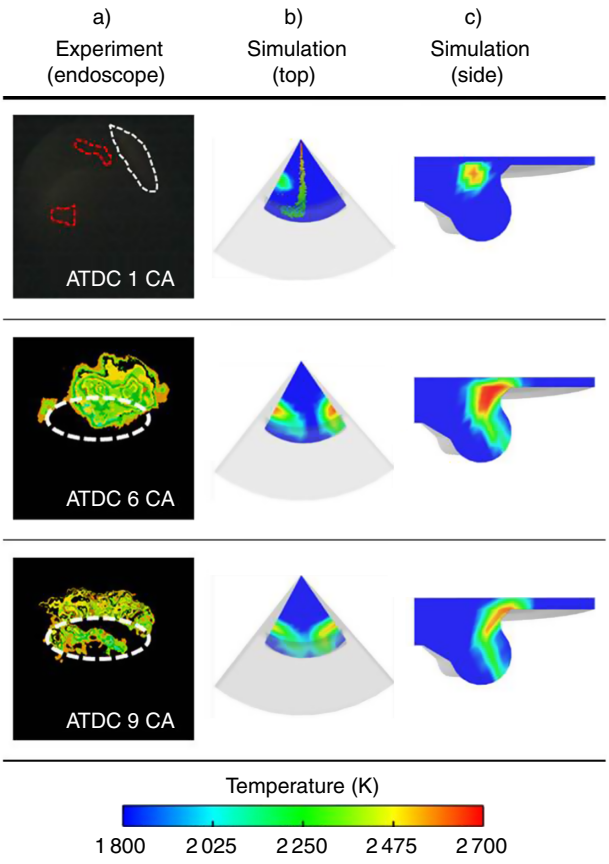

Figure 3

Comparison of spray and temperature distribution between the experiment and simulation for ULSD combustion.

happened at the same time as that of the experimental case.

The endoscopic images show the behavior of spray and combustion in the combustion chamber. Figure 3 represents the spray and temperature distribution of the ULSD pilot injection (BTDC 60 CA and 10 CA) case, compared with the KIVA results under the same conditions. The first image in the left column captured the main spray jet and sparks. The white dashed line outlines the main spray jet and the red dashed line indicates sparks which were the ignition source of the main combustion. In the second and third columns (simulation contour), the same patterns were observed with regard to spray and temperature characteristics. As can be seen in the first images of all columns, the high-temperature region appeared at the outer spray jet, which was induced by a rapidly forming mixture between fuel droplets and charged air in the middle of the jet stream. The images in the first column were obtained using the ThermoVision program, and illustrate temperatures from 1 800 K to 2 700 K. Flame temperature distribution images are shown in the second and third pictures. There is a piston bowl center in the endoscopic pictures that is expressed by the white dashed line. USLD combustion was mainly developed near the piston lip and bowl in the experimental case. For the numerical case, the high combustion temperature region occupied the same position.

Due to the fact that DME fuel has no carbon-to-carbon bond in the chemical structure, it is not possible to detect the DME flame and temperature distribution using the visualization system [7]. However, a numerical approach can allow flame and temperature analysis with accurate prediction capability. The above verified numerical model was also used in the DME combustion study and it distinctly showed the effects of pilot injection strategies on DME combustion characteristics including temperature distributions.

2.2 Combustion Characteristics of Pilot Injection

Figure 4 shows the combustion pressure and the heat release rate for DME and ULSD fuels under various pilot injection timings. As can be seen in Figure 4, the first injected fuel increased the in-cylinder pressure and temperature before the main combustion started. Although pilot combustion events were observed at the same time regardless of the first injection timing, they affected combustion pressure differently at the time when the main combustion events began. For the case of BTDC 15 CA (main injection) in Figure 4a, DME combustion shows similar combustion characteristics regardless of pilot timings. This is because the main oxidation was started before the formation of the high pressure and temperature in the combustion chamber by the pilot combustion. The active fuel evaporation rate of DME led to an air/fuel mixture forming a short time after the fuel was injected into the chamber. As a result, the ignition delay seemed shorter and the premixed combustion phase occurred dominantly compared with those of ULSD fuel. On the other hand, the effect of the pilot injection timing on ULSD main combustion was observed, as seen in Figure 4a. When the pilot fuel was injected earlier, the longer air and fuel mixing time made more homogeneous mixtures, which caused the discrepancy of the auto-ignition starting points and the peak of combustion pressure.

As shown in Figure 4b, c, it can be observed that the pilot timing resulted in contrary combustion behavior between DME and ULSD fuels. When the pilot injection timing was retarded in the DME combustion case, higher in-cylinder pressure and a shorter ignition delay

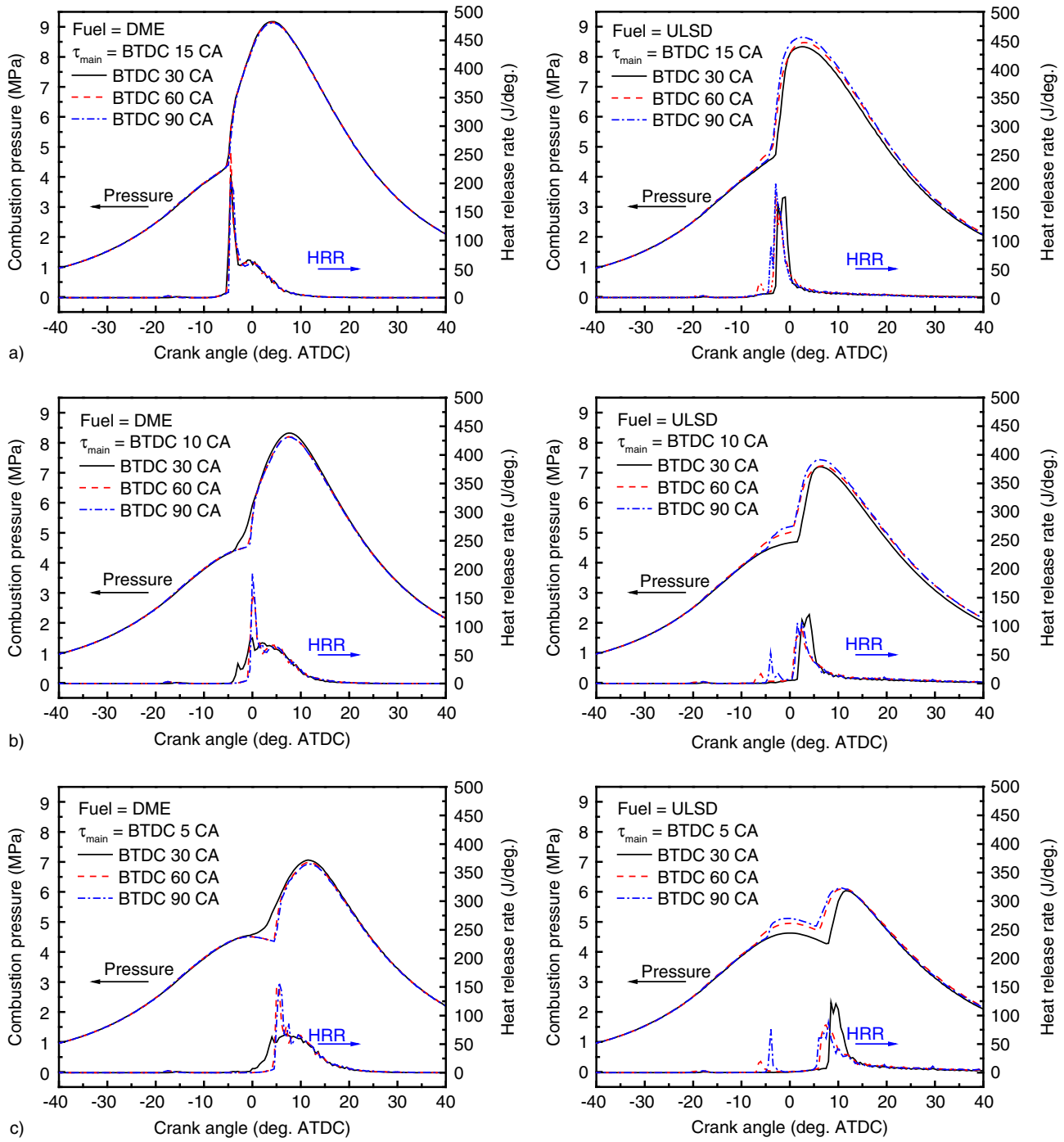

Figure 4

Combustion pressure and heat release rate of various pilot injection timings for DME and ULSD fuels (main injection timing at: a) BTDC 15 CA, b) BTDC 10 CA, and c) BTDC 5 CA).

were observed in the main combustion processing. On the other hand, the peak pressure and ignition delay of ULSD combustion were lower and longer, respectively. Due to the fact that the fast oxidation reaction of the DME fuel suppressed the influence of earlier pilot injections, advanced pilot timings (BTDC 90 CA and 60 CA) caused a similar result in the single-injection case. Whereas, the oxidation of the fuel injected at

BTDC 30 CA continued until the second combustion started, which induced an increased combustion pressure and lower premixed heat release rate.

Although the mass for the pilot injection was fixed at 2 mg in all cases, the ULSD pilot combustion shows strong effects, as seen in the pressure-heat release rate-crank angle diagram. In comparison with the DME properties, the ULSD shows poor atomization and long ignition delay characteristics. For DME fuel properties, low boiling temperature and high vapor pressure make it a gaseous state under lower pressure conditions [13]. Thus, liquefied DME fuel which is pressurized during the injection into the combustion chamber evaporates fast after fuel is emitted from the injector. When DME fuel turns into the gaseous state, the formation of the fuel/air mixture is accelerated and then the ignition starts fast. In addition, the high cetane number (>55) and oxygen contents in the DME lead to a better compression-ignition quality and short ignition delay [21]. On the other hand, the evaporation rate of ULSD fuel is lower and fuel breakup processing takes more time than those of DME fuel. Although the gas oil boils in low temperature conditions (~248 K), the conventional Diesel fuel vaporizes under high ambient temperature (over 450 K), which suppresses the atomization response relatively.

These features of ULSD fuel induced a two-stage combustion phenomenon. One part of the fuel injected in the first step was consumed at around BTDC 18 CA, and the other, which was left in the squish region, was burned rapidly at the end of the compression process. This pilot combustion made the in-cylinder pressure higher than the motoring pressure, thereby shortening the ignition delay of the main injection. In addition, the combustion pressure and the heat release rate had a high peak value during the first-stage combustion because the earliest pilot timing case took a long time to form homogeneity in the fuel-air mixture.

As can be seen in Figure 4, the dwelling time between the pilot and the main injection strongly influenced the combustion characteristics. Figure 4a shows that the advanced main timing dominantly produced a premixed combustion phase. This is because the unburned air-fuel mixture from the first stage was oxidized with the injected fuel from the second injection. When the dwelling time increased, the peak value of the heat release rate in the main combustion event decreased for the ULSD due to the fact that most of the pilot fuel was consumed before the main combustion. For the DME fuel, the well-mixed fuel/air mixtures by the aforementioned fuel properties induced a high premixed combustion phase.

The development of the spray procedure and the equivalence ratio in the pilot injection is illustrated in Figure 5. It is confirmed that the better atomization

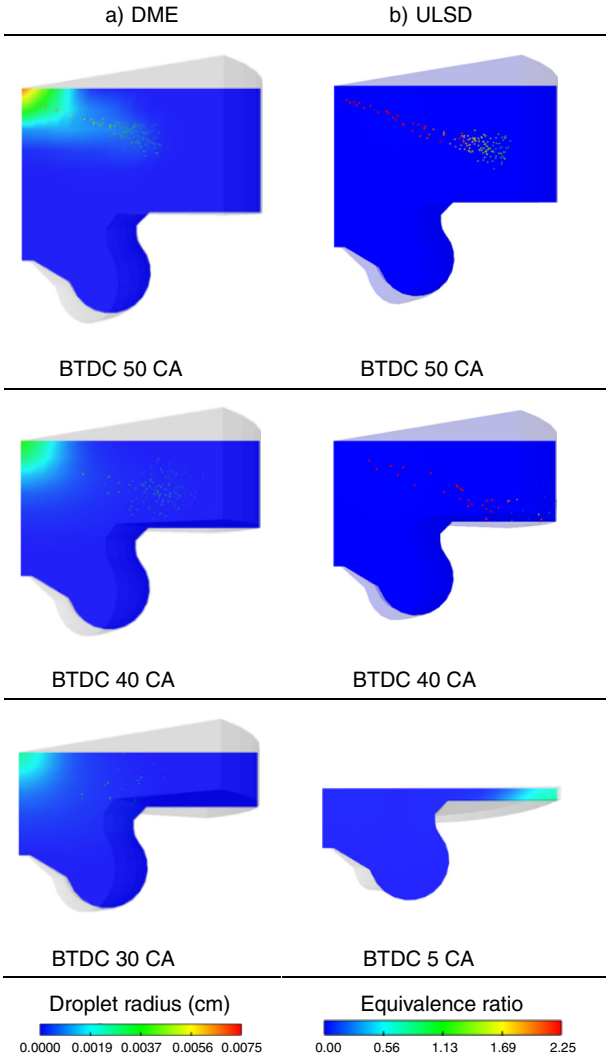

Figure 5

Pilot spray development process and equivalence ratio distribution with respect to the crank angle (τ_{pilot} = BTDC 60 CA, τ_{main} = BTDC 10 CA).

characteristics of the DME fuel than the ULSD fuel result in smaller droplet particles and a higher equivalence ratio region downstream of the spray jet. These easily broken particles quickly formed a fuel-rich area, mixing with the ambient air. As can be seen in Figure 5b, however, particles which had a large size penetrated farther into the combustion chamber and arrived at the squish area. Moreover, the fuel-rich mixture by the pilot injection appeared at the end of the squish zone in the later time due to the poor atomization properties of the ULSD fuel. During the compression process,

the pressure in the narrow squish space was increased to ignite the fuel-air mixture, which allowed an interesting thing to happen in the ULSD cases: two fast pilot fuels were burned at the same timing (around BTDC 7 ~ 5 CA) in different main timings, as shown in Figure 4. Such fuels formed their mixture at similar squish areas even under various main injection conditions, which generated the same ignition timing. However, the BTDC 90 CA condition showed a high heat release rate due to longer mixing time.

2.3 Combustion Temperature Distribution

The comparison of the temperature distribution for DME and ULSD fuels during the combustion process is illustrated in Figure 6. As there are no carbon-to-carbon bonds in the chemical structure of DME, the combustion temperature distribution is unable to be detected by the experimental equipment. However, it can be predicted by the KIVA code. The main DME combustion started at the side of the spray jet and at an earlier time than ULSD. Furthermore, the combustion process developed rapidly following the trace of the spray penetration. This active combustion characteristic was caused by a good atomization process and oxygen contents in the DME fuel. A high temperature zone spread widely in a short time when the DME fuel burned. On the contrary, the ULSD combustion reaction was observed at the piston lips where the spray impinged. Despite a smaller quantity of ULSD than DME fuel, a slow break-up process generated a longer penetration length and relatively low combustion temperature. For the ULSD combustion temperature, the small amount of entrained air was used for oxidation in the restricted region (at the end of the injection fuel jet) where the premixed fuel-air mixture was contained, resulting in decreased combustion temperatures, as can be seen in Figure 7a. In the average temperature diagram, it shows that the ULSD temperature increased faster and had a lower peak value compared with that of the DME fuel. Although the combustion starting point of DME was advanced, the ULSD temperature increased faster and higher because of the strong pilot combustion.

Figures 7b and 8 represent the effects of the pilot timing on the average temperature and the combustion temperature distribution with top and side views. The injection conditions state that the main injection timing was at BTDC 5 CA, and pilot timings from BTDC 90 CA to BTDC 30 CA in 30 CA steps were employed. There was little difference in temperature values between the BTDC 90 CA and BTDC 60 CA conditions. For comparison of the two pilot injection

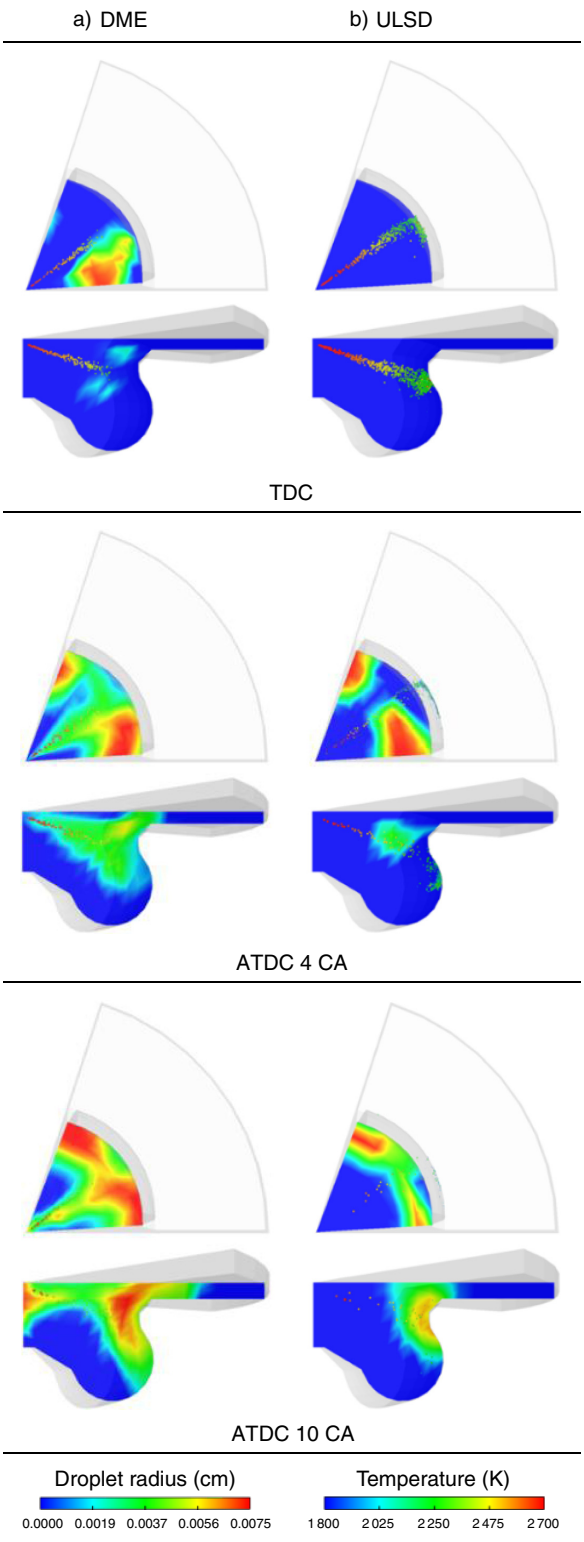

Figure 6

The development of combustion and temperature distribution for DME and ULSD fuels at the τ_{pilot} = BTDC 60 CA and τ_{main} = BTDC 10 CA.

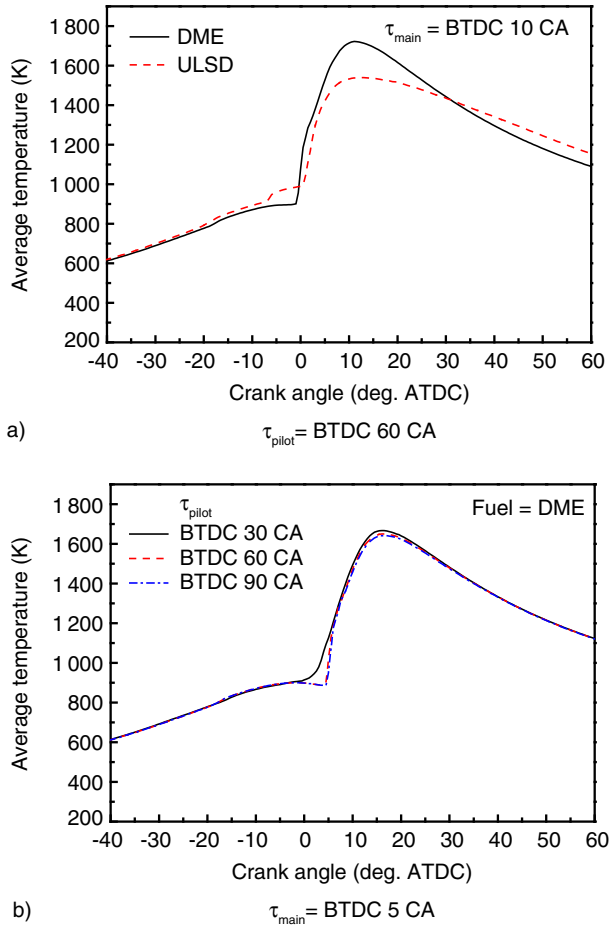

Figure 7

Effect of: a) fuel types and b) pilot injection timings on the average combustion temperature.

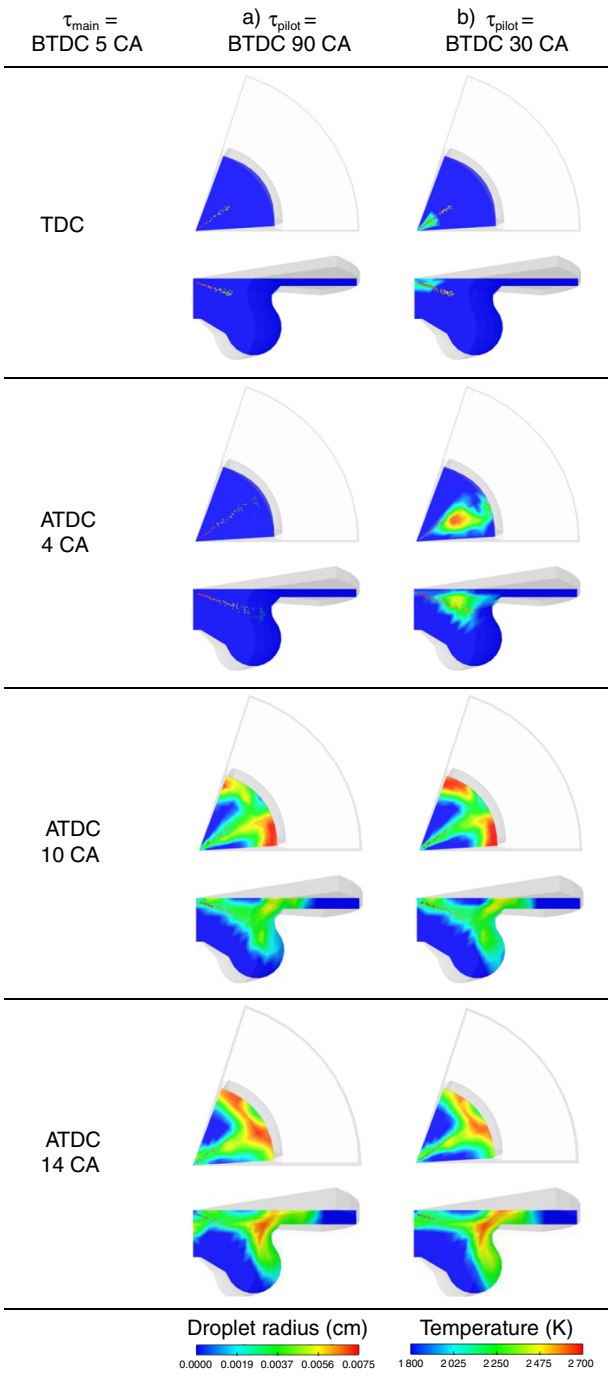

Figure 8

Effect of the pilot injection timing on combustion temperature distribution of DME fuel at τ_{main} = BTDC 5 CA.

conditions (BTDC 90 CA and BTDC 30 CA), the effect of pilot injection appeared in terms of the combustion temperature value and distribution. The retarded pilot timing case had an earlier combustion starting point and higher temperature during the entire combustion process. In Figure 8b, it also shows that the oxidation reaction of the retarded injection case emerged from the nozzle tip with the premixed mixture. On the other hand, the combustion event occurred late in the advanced injection case. After ATDC 10 CA in Figure 8, the temperature contours show very similar patterns between the two different timing conditions, with slightly different range of temperature values. This difference can be explained by the change in pilot injection timings causing different injection targeting points. As a result, the injection at BTDC 90 CA was spread out at the squish region, mixing with ambient air uniformly before the main fuel was injected. The first injected fuel in the BTDC 30 CA case was distributed to the squish

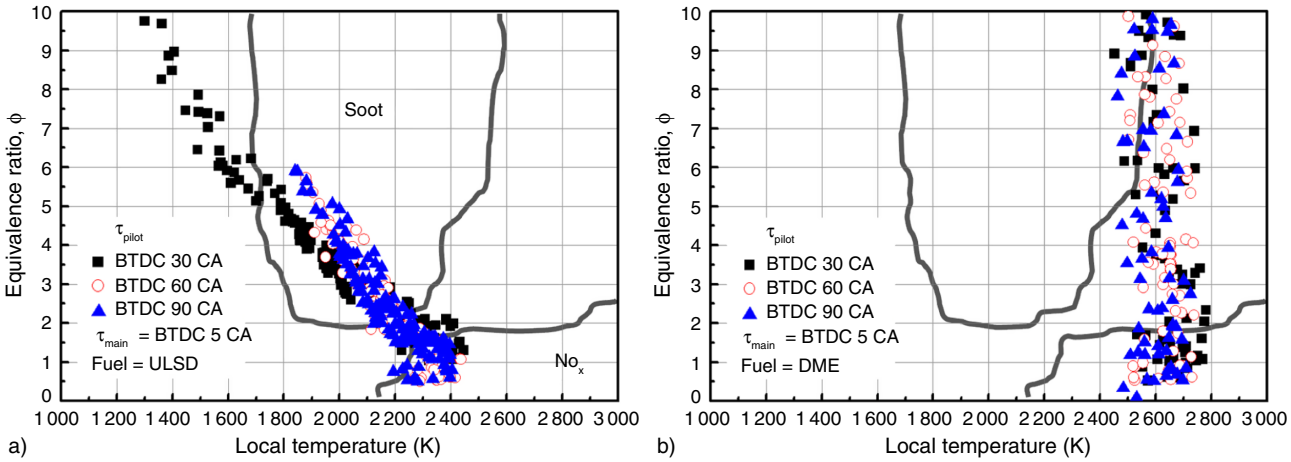

Figure 9

NO_x and soot emission of various pilot injection conditions related to the equivalence ratio and local temperature for: a) ULSD and b) DME fuels.

area and the piston bowl region, which formed a fuel-rich region in the piston bowl. The high equivalence ratio zone generated the main ignition with a high temperature, as illustrated in Figure 8b.

2.4 Exhaust Emission Characteristics

Figure 9 shows that the pilot injection timings affected exhaust emissions such as NO_x and soot on the Φ (equivalence ratio) – T (temperature) map. Each point represents the Φ and T values of calculated cells obtained from the KIVA-3 V at the crank angle at 90% of the maximum heat release rate. The Φ – T map has been widely used to theoretically analyze the effect of the equivalence ratio and local temperature on combustion products [22, 23]. Akihama *et al.* [24] expanded the concept of the Φ – T map for the investigation of smokeless Diesel combustion performing 0-D calculations, which was introduced as a reference guideline in this study. The solid line in Figure 9 indicates the soot formation region (shape of a peninsula) and NO_x formation region (right bottom corner), respectively. Furthermore, the concentration of each emission is increased when moving toward the center of the solid line.

As illustrated in Figure 9b, combustion products of the DME fuel occupied the high NO_x region and soot-free region. As described above, due to the fact that there is no carbon-to-carbon bond in the chemical structure, DME combustion rarely creates soot emissions. Moreover, it was revealed that the oxygen content in the fuel and its lean-burn condition generate a high combustion temperature (2 500 K < T < 2 800 K) and suppress soot formation. Due to high fuel-rich mixture cells, the ULSD combustion had relatively lower local temperature values and occupied the high soot formation area. Additionally, these low temperatures and the high soot area resulted in a small amount of NO_x emissions and a high concentration of soot emissions in the ULSD combustion.

The effect of the pilot injection timing on emissions is also represented in Figure 9 when the main injection timing was BTDC 5 CA and pilot injection timings were from BTDC 90 CA to BTDC 30 CA The retarded pilot timing condition shows a slightly higher temperature for both fuels. Especially, the BTDC 30 CA case in the ULSD combustion has a wide range of equivalence ratios and local temperatures. This is because the first injected fuel does not have sufficient time to be mixed with the charged air. On the other hand, the results of the other conditions are gathered in a specific range with 0 < Φ < 6 and 1 800 K < T < 2 400 K. Pre-combustion reduced the main combustion temperature as well as premixing the first injection, which did not form a fuel-rich mixture.

CONCLUSIONS

This numerical investigation was performed to verify the effects of various pilot injection timings on the combustion behavior of DME and ULSD fuels in terms of combustion pressure, heat release rate, and temperature

distribution, which were undetectable in the experimental approach. To heighten the accuracy of the simulation, model validation compared with the experimental results was conducted and showed good agreement. The KIVA-3 V code implemented numerical experiments of various injection conditions fueled with DME and ULSD and drew the results as follows:

1. The span between the pilot injection timing and the main timing strongly affected combustion characteristics. With a short span the advanced main timing (BTDC 15 CA) decreased the influence of the pilot injection to start the main combustion before pilot oxidation reacted. In contrast, a retarded second injection condition initiated under high ambient pressure and temperature decreased the peak combustion pressure and heat released by the first combustion;
2. Due to different fuel properties for DME and ULSD fuels, an opposite trend of combustion pressure and heat release rate occurred. Pilot-injected fuel formed a fuel-air mixture at different positions in the combustion chamber according to the test fuels. As a result, the first combustion occurred in different areas;
3. DME combustion occurred in a wide range of areas within the combustion chamber, with a higher combustion temperature compared with ULSD combustion. Although the pilot injection led to the change in the main ignition timing and temperature spectrum values, the overall temperature distribution pattern was determined by the main combustion;
4. The production of NO_x and soot emissions is represented on the expanded $\Phi - T$ map. DME combustion occupies soot-free combustion and high-temperature regions, which also suppressed the formation of soot emissions. On the other hand, ULSD combustion included high soot formation conditions and a low-temperature region in which a low concentration of NO_x is produced. Retarded pilot timing cases had a slightly higher local temperature than other conditions.

ACKNOWLEDGMENTS

This work (2012R1A2A2A01046859) was supported by Mid-career Researcher Program through NRF (National Research Foundation) grant funded by the MSIP (Ministry of Science, ICT and Future Planning).

REFERENCES

1 Teng H., McCandless J.C., Schneyer J.B. (2004) Thermodynamic properties of dimethyl ether – an alternative fuel for compression-ignition engines, *SAE Tech. Paper* 2004-01-0093.

2 Kim M.Y., Yoon S.H., Ryu B.W., Lee C.S. (2008) Combustion and emission characteristics of DME as an alternative fuel for compression ignition engines with a high pressure injection system, *Fuel* **87**, 2779-2786.

3 Sato Y., Nozaki S., Noda T. (2004) The Performance of Diesel Engine for Light Duty Truck Using a Jerk Type In-Line DME Injection System, *SAE Tech. Paper* 2004-01-1862.

4 An B., Sato Y., Lee S.W., Takayanagi T. (2004) Effects of Injection Pressure on Combustion of a Heavy Duty Diesel Engine with Common Rail DME Injection Equipment, *SAE Tech. Paper* 2004-01-1864.

5 Yoon H., Yeom K., Bae C. (2007) The Effects of Pilot Injection on Combustion in Dimethyl-ether (DME) Direct Injection Compression Ignition Engine, *SAE Tech. Paper* 2007-24-0118.

6 Song R., Li K., Feng Y., Liu S. (2009) Performance and Emission Characteristics of DME Engine with High Ratio of EGR, *Energ. Fuel.* **23**, 5460-5466.

7 Jeon J., Kwon S.I., Park Y.H., Oh Y., Park S. (2014) Visualizations of combustion and fuel/air mixture formation processes in a single cylinder engine fueled with DME, *Appl. Energ.* **113**, 294-301.

8 Amsden A.A. (1993) KIVA-3: A KIVA program with block-structured mesh for complex geometries, *Los Alamos National Laboratory Report* LA-12503-MS.

9 Amsden A.A. (1997) KIVA-3 V: A block-structured KIVA program for engines with vertical or canted valves, *Los Alamos National Laboratory Report* LA-13313-MS.

10 Kee R.J., Rumpley F.M., Miller J.A. (1989) CHEMKIN-II: A Fortran chemical kinetics package for the analysis of gas phase chemical kinetics, *Sandia National Laboratory Report* SAND89-8009.

11 Reitz R.D. (1987) Modeling atomization processes in high-pressure vaporizing sprays, *Atomization Spray.* **3**, 309-337.

12 Han Z., Reitz R.D. (1995) Turbulence modeling of internal combustion engines using RNG k-ε models, *Combust. Sci. Technol.* **106**, 267-295.

13 Teng H., McCandless J.C., Schneyer J.B. (2001) Thermochemical characteristics of dimethyl ether – an alternative fuel for compression-ignition engines, *SAE Tech. Paper* 2001-01-0154.

14 Teng H., McCandless J.C., Schneyer J.B. (2002) Viscosity and lubricity of (liquid) dimethyl ether – an alternative fuel for compression-ignition engines, *SAE Tech. Paper* 2002-01-0862.

15 Teng H., McCandless J.C., Schneyer J.B. (2003) Compression ignition delay (physical + chemical) of dimethyl ether – an alternative fuel for compression-ignition engines, *SAE Tech. Paper* 2003-01-0759.

16 Teng H., McCandless J.C. (2005) Comparative study of characteristics of Diesel-fuel and dimethyl-ether sprays in the engines, *SAE Tech. Paper* 2005-01-1723.

17 Patel A., Kong S.C., Reitz R.D. (2004) Development and validation of a reduced reaction mechanism for HCCI engine simulation, *SAE Tech. Paper* 2004-01-0558.

18 Kong S.C., Sun Y., Reitz R.D. (2007) Modeling Diesel spray flame liftoff, sooting tendency, and NO_X emissions using detailed chemistry with phenomenological soot model, *J. Eng. Gas Turb. Power* **129**, 245-251.

19 Patterson M.A., Kong S.C., Hampson G.J., Reitz R.D. (1994) Modeling the effects of fuel injection characteristics on Diesel engine soot and NO_X emissions, *SAE Tech. Paper* 940523.

20 Schmidradler D., Werlberger P. (1999) Engine Videoscope Thermovision: Vision Based Temperature Measurement for Diesel Engine, *ISATA 99ME039*.

21 Gill D., Ofner H. (1999) DiMethyl Ether – a clean Fuel for Transportation, *SAE Tech. Paper* 990059.

22 Kmimoto T., Bae M. (1988) High Combustion Temperature for the Reduction of Particulate in Diesel Engines, *SAE Tech. Paper* 880423.

23 Neely G.D., Sasaki S., Huang Y., Leet J.A., Stewart D.W. (2005) New Diesel Emission Control Strategy to Meet US Tier 2 Emissions Regulations, *SAE Tech. Paper* 2005-01-1091.

24 Akihama K., Takatori Y., Inagaki K., Sasaki S., Dean A.M. (2001) Mechanism of the Smokeless Rich Diesel Combustion by Reducing Temperature, *SAE Tech. Paper* 2001-01-0655.

Manuscript accepted in June 2014
Published online in September 2014

Cite this article as: J. Jeon, Y.H. Park, S. Il Kwon and S. Park (2014). Effect of Pilot Injection Timings on the Combustion Temperature Distribution in a Single-Cylinder CI Engine Fueled with DME and ULSD, *Oil Gas Sci. Technol* **71**, 15.